Research Paper

Noninvasive Imaging of CD206-Positive M2 Macrophages as an Early Biomarker for Post-Chemotherapy Tumor Relapse and Lymph Node Metastasis

Chenran Zhang[1], Xinhe Yu[1], Liquan Gao[1], Yang Zhao[1], Jianhao Lai[1], Dehua Lu[1], Rui Bao[1], Bing Jia[1, 2], Lijun Zhong[2], Fan Wang[1, 3], Zhaofei Liu[1✉]

1. Medical Isotopes Research Center and Department of Radiation Medicine, School of Basic Medical Sciences, Peking University Health Science Center, Beijing 100191, China;
2. Medical and Healthy Analytical Center, Peking University, Beijing 100191, China;
3. Key Laboratory of Protein and Peptide Pharmaceuticals, CAS Center for Excellence in Biomacromolecules, Institute of Biophysics, Chinese Academy of Sciences, Beijing 100101, China.

✉ Corresponding author: Zhaofei Liu, Ph.D., Medical Isotopes Research Center and Department of Radiation Medicine, School of Basic Medical Sciences, Peking University Health Science Center, Beijing 100191, China. Phone: +86-1082802871; E-mail: liuzf@bjmu.edu.cn.

Abstract

Tumor relapse after initial regression post-chemotherapy is a major challenge in cancer treatment, as it usually leads to local-regional recurrence or inoperable distant metastasis. M2 macrophages diminish the tumor-inhibitory effect of chemotherapy and correlate with distant metastasis and poor prognosis. In this study, we investigated whether molecular imaging of M2 macrophages could serve as an early biomarker for tumor relapse after chemotherapy and tumor lymph node metastasis in preclinical mouse models. **Methods:** We developed M2 macrophage-targeted probes for near-infrared fluorescence (NIRF) imaging and single-photon emission computed tomography (SPECT) using an anti-CD206 monoclonal antibody. The specific targeting capacity and potential applications of the NIRF and SPECT probes were investigated in subcutaneous tumor and lymph node metastasis models of 4T1 murine breast cancer. **Results:** M2 macrophage infiltration was significantly increased in the 4T1 tumors that later underwent relapse but not in non-relapsing 4T1 tumors after cyclophosphamide treatment. Through NIRF imaging and SPECT using our synthesized probes, the infiltration of M2 macrophages in relapsing tumors and tumor lymph node metastasis could be sensitively detected. Importantly, early prediction of tumor relapse by molecular imaging of M2 macrophages resulted in an effective eradication of tumors upon combination with additional radiotherapy. **Conclusion:** Our findings demonstrate that M2 macrophage-targeted imaging allows for noninvasively predicting post-chemotherapy tumor relapse and sensitively detecting the metastatic lymph nodes *in vivo*. This imaging strategy could provide a better understanding of cancer progression, enable early prediction of tumor resistance, and have implications on the rational design of cancer therapeutics.

Key words: M2 macrophage, CD206, Molecular imaging, SPECT, Tumor resistance.

Introduction

Despite advances in oncology research, cancer-related deaths remain one of the leading causes of mortality worldwide. One of the major reasons for high cancer mortality and treatment failure in patients is tumor recurrence after treatment of the primary tumor by either surgery or traditional therapies such as chemotherapy and radiotherapy [1, 2]. Tumor relapse after initial regression is a major challenge for cancer therapy, as it often leads to local-regional recurrence or inoperable distant metastasis, and over 90% of cancer-related deaths currently result from metastatic disease and related complications [3, 4]. Therefore, early detection of biomarkers predictive of tumor relapse and

metastasis could enable enhanced prediction of tumor resistance to therapy, provide alternative treatment strategies, and facilitate improved cancer management.

Solid tumors include not only tumor cells, but also the stroma, which consists of an extracellular matrix, tumor vasculature, and immune cells that shape the tumor microenvironment [5]. Macrophages are a major component of murine and human tumor stromal cells [6], which infiltrate into tumors from the peripheral blood and differentiate from monocyte precursors [3]. Tumor infiltrating macrophages are commonly termed tumor-associated-macrophages (TAMs). Macrophages adopt distinct phenotypes influenced by the microenvironment, defined as "classically activated" M1-type and "alternatively activated" M2-type. TAMs generally express an M2-like phenotype with tumor promoting functions [7]. Clinical evidence has shown that high TAM numbers correlate with poor prognosis in patients with various cancers [8].

TAMs play an essential role in tumor progression by stimulating angiogenesis, tumor cell invasion and metastasis, and suppressing anti-tumor immunity [3]. Therefore, detection of M2 macrophages (TAMs) within the tumor microenvironment can lead to improved outcomes by providing opportunities for monitoring tumor progression. Macrophage mannose receptor (MMR), or CD206, is highly expressed on M2 macrophages but not on M1 macrophages [9, 10]. Molecular imaging of CD206 has been successfully investigated for the noninvasive detection of M2 macrophages *in vivo* [11-13], and M2 macrophage depletion has been shown to inhibit tumor growth and metastasis, and enhance the efficacy of anti-tumor therapy [14-16].

Chemotherapy is a frontline cancer therapy, especially for patients who are not eligible for surgery. However, tumor recurrence after chemotherapy threatens the survival of cancer patients. Several studies found that chemotherapeutic drugs increase M2 macrophage recruitment to tumors [2, 17]. Increased M2 macrophage infiltration stimulates tumor relapse after chemotherapy by promoting vascular reconstruction and immunoregulation [2, 17-19]. Therefore, M2 macrophage is a potential target to evaluate and predict post-chemotherapy tumor relapse and metastasis.

Molecular imaging techniques such as positron emission tomography (PET), single-photon emission computed tomography (SPECT) and near-infrared fluorescence (NIRF) imaging provide a noninvasive way to image biological processes *in vivo* [20, 21]. In this study, we investigated whether CD206-targeted molecular imaging of M2 macrophages could be used for the identification of early tumor relapse after chemotherapy as well as tumor lymph node metastasis in preclinical mouse models.

Materials and Methods

Animal models

The 4T1 murine breast cancer cell line was obtained from the American Type Culture Collection and cultured as previously described [11]. Firefly luciferase stably-transfected 4T1 (4T1-fLuc) cells were generated and cultured as previously described [22]. Female BALB/c normal mice (5 weeks of age) were purchased from Department of Laboratory Animal Science, Peking University. All animal studies were performed in accordance with the Guidelines of Peking University Animal Care and Use Committee. To establish a subcutaneous 4T1 tumor mouse model, female BALB/c mice were subcutaneously injected with 1×10^6 4T1 cells into the right hind legs. Tumor growth was measured using a caliper, and tumor volume was calculated using the formula: volume = length × width^2/2.

For development of a lymph node metastasis mouse model, 2×10^5 4T1-fLuc cells were injected into the right hind footpads of female BALB/c mice [23]. The growth of lymph node metastatic tumors was monitored by bioluminescence imaging (BLI) of anesthetized mice using an *in vivo* IVIS optical imaging system (Xenogen, Alameda, CA) starting from 10 min after D-luciferin administration (150 mg/kg by intraperitoneal injection).

Cyclophosphamide treatment

Cyclophosphamide (CTX) treatment started when the 4T1 tumor-bearing mice reached a tumor volume of 100–150 mm^3. Mice were separated into 3 groups (n =15 or 20 per group), and were intraperitoneally administered CTX (in phosphate buffered solution; PBS) at a single dose (150 mg/kg, once on day 0) or multiple doses (75 mg/kg, on days 0, 3, 6, 9, 12, and 15), or PBS only (vehicle control). On day 8, three mice from each group were euthanized. Tumors were harvested, cut into 8 μm thick frozen sections, and stained for mouse CD206 and F4/80. Meanwhile, 5 mice from each group were euthanized, and their tumors were enzymatically digested using a previously described method [16] to obtain single-cell suspensions for flow cytometry analysis. On day 32, mice from each group (n = 6 or 8 per group) were euthanized. The lungs were filled with 15% India ink via the upper trachea and fixed in Fekete's solution (100 mL of 70% alcohol, 10 mL of 4% formalin, and 5 mL of glacial acetic acid) for 48 h. Metastatic lesions,

which appeared as white nodules on the lung surface, were counted and photographed.

In a separate experiment, 4T1 tumor-bearing BALB/c mice were treated with PBS, a single dose of CTX (150 mg/kg, once on day 0), or multiple doses of CTX (75 mg/kg, on days 0, 3, and 6). On day 7, five mice from each group were subjected to CD206-targeted NIRF imaging as described below. On day 8, three mice from each group were subjected to CD206-targeted SPECT/CT imaging and five mice from each group were subjected to a biodistribution analysis, respectively, as described below.

Flow cytometry analysis

Single-cell suspensions were incubated with phycoerythrin (PE)-conjugated rat anti-mouse F4/80 (clone BM8; Sungene, Tianjin, China) and fluorescein isothiocyanate (FITC)-conjugated rat anti-mouse CD206 antibodies (clone C068C2; Sungene, Tianjin, China) for 1 h at 4°C, then analyzed using a FACSCalibur LSR-II flow cytometer (Becton Dickinson, Germany).

Preparation of CD206-targeting probes

The CD206-targeting NIRF probe was generated using a previously described method [16]. Briefly, anti-CD206 antibody (αCD206, clone C068C2, IgG2a; Biolegend, San Diego, CA) was mixed with Dylight755-N-hydroxysuccinimide (NHS) ester (Pierce, Rockford, IL) in sodium bicarbonate buffer (pH 8.4) at a 1:10 molar ratio. After incubation for 12 h at 4°C, the mixture was purified using a PD-10 desalting column (GE Healthcare, Piscataway, NJ). The degree of labeling (dye/protein molar ratio) of Dylight755-αCD206 (Dye-αCD206) was 6:1, as detected using an ultraviolet spectrophotometer (Thermo Fisher Scientific, Waltham, MA). Dylight755-labeled isotype-matched control rat IgG (Dye-IgG) was synthesized as a control using the same method.

The CD206-targeting radiotracer was generated by radiolabeling anti-CD206 antibody (100 μg) with 185 MBq Na[125]I using a previously described method [24]. Briefly, 100 μg of antibody dissolved in 0.2 M PBS (pH 7.4) was mixed with 185 MBq of Na[125]I in a vial pre-coated with Iodogen (Sigma, St. Louis, MO). After incubating at room temperature for 10 min, the product, ^{125}I-αCD206, was purified using a PD-10 desalting column. The radiochemical purity of ^{125}I-αCD206 was >98%. ^{125}I-labeled isotype-matched IgG (^{125}I-IgG) was also prepared using the same method.

In vivo NIRF imaging

For *in vivo* CD206-targeted NIRF imaging, each 4T1 tumor-bearing mouse was intravenously (i.v.) administered 0.5 nmol of Dye-αCD206 or control Dye-IgG. At 4, 24, 48, 72, and 96 h postinjection (p.i.), mice (n = 5 per group) were imaged using a Maestro In-Vivo Imaging System (CRI, Woburn, MA). For each scan, aliquots containing a known amount of injectate were imaged. Images were acquired and analyzed using Maestro 2.4 software (CRI, Woburn, MA). Tumor uptake was determined by normalizing the fluorescence intensity of the tumor by the dose of injected probe [25].

Small-animal SPECT/CT and biodistribution

Mice were i.v. administered 25.9 MBq of ^{125}I-αCD206 (~16 μg) or ^{125}I-IgG (n = 3 per group). SPECT and helical CT scans were performed at 24 h p.i. with a NanoScan SPECT/CT system (Mediso, Budapest, Hungary) using a previously described protocol [26, 27].

For biodistribution analysis, 4T1 tumor-bearing mice were i.v. injected with 0.296 MBq of ^{125}I-αCD206 (~0.2 μg) or ^{125}I-IgG (n = 5 per group). At 24 h p.i., mice were euthanized, and blood, tumors, major organs were collected and weighed. Tissue radioactivity was measured using a γ-counter (Packard, Meriden, CT). Results are presented as a percentage of the injected dose per gram of tissue (%ID/g).

Additional radiotherapy

4T1 tumor-bearing BALB/c mice were treated with PBS (n = 5) or a single dose of CTX (150 mg/kg in PBS, once on day 0; n = 18). The CTX-treated mice were then separated into 3 groups (n = 6 per group): additional radiotherapy on days 8 and 9; additional radiotherapy on days 14 and 15; and without additional radiotherapy. For each radiotherapy, the 4T1 tumors were locally irradiated with 6 Gy [28] using an X-ray irradiator (Rad Source Technologies, Suwanee, GA). At the end of the study (day 28), mice were euthanized and tumors were harvested, weighed, and photographed.

M2 macrophage sorting and transplantation

F4/80+CD206+ M2 macrophages were sorted from a single cell suspension on day 9 harvested from donor 4T1 tumor-bearing BALB/c mice treated with a single dose of CTX (150 mg/kg) on day 0. For the macrophage transplantation experiment, acceptor 4T1 tumor-bearing mice treated with multiple doses of CTX (75 mg/kg, on days 0, 3, 6, and 9) received either 2 × 10^5 F4/80+CD206+ macrophages or PBS by a 25 μL intratumoral injection [2] on day 10. Tumor growth was monitored every other day. On day 20, three mice from each group were euthanized. Tumors were harvested and cut into 8 μm thick frozen sections for histological analysis of Ki67. At the end of the study

(day 24 for control group, and day 32 for CTX-treated groups), mice from each group (n = 5 per group) were euthanized, and metastatic lesions in the lungs were examined using the protocol described above. The lungs were also embedded in paraffin, cut into sections, and stained with hematoxylin and eosin (H&E).

Noninvasive imaging of lymph node metastasis

To investigate the potential of CD206-targeted imaging for the noninvasive detection of tumor lymph node metastasis, BALB/c mice inoculated with 4T1-fLuc tumors in the footpad were subjected to Dye-αCD206 NIRF imaging or ^{125}I-αCD206 SPECT/CT on day 7 or day 9 after 4T1-fLuc cell inoculation. After the imaging studies, both left and right popliteal lymph nodes were exposed and surgically harvested. *In vivo* imaging was subsequently repeated to evaluate the residual imaging signals. BLI was performed throughout the study for comparison. For further confirmation of tumor lymph node metastasis, surgically-excised lymph nodes were fixed and subjected to both immunofluorescence staining and H&E staining.

Immunofluorescence staining

The immunofluorescence staining experiments were performed, and the staining results were analyzed by two investigators (L.G. and Y.Z.) who were blinded to the results of flow cytometry, *in vivo* imaging, and tumor therapy. For CD206 and F4/80 analyses, frozen sections were incubated with rat anti-mouse CD206 (1:100; clone C068C2, IgG2a; Biolegend, San Diego, CA) and rabbit anti-mouse F4/80 antibodies (1:100; ab74383; Abcam, Cambridge, MA) and then visualized using Dylight549- or FITC-conjugated secondary antibodies (1:200; Earthox, Millbrae, CA) under a confocal microscope (Leica, Wetzlar, Germany). For Ki67 analysis, frozen sections were incubated with rabbit anti-mouse Ki67 (1:100; AB9260; Millipore, Billerica, MA) and then visualized using a Dylight549-conjugated secondary antibody (1:200; Earthox, Millbrae, CA). The tumor cell proliferation index was calculated as the percentage of Ki67-positive nuclei among the total number of nuclei.

Statistical analysis

Quantitative data are shown as mean ± SD. Data were analyzed using GraphPad Prism version 6.0 (GraphPad Software, San Diego, CA). Statistical analysis was done using a 1-way ANOVA and an unpaired Student *t* test. *P* values < 0.05 were considered statistically significant.

Results

Increased recruitment of M2 macrophages in CTX-treated tumors before relapse

To investigate whether CD206-positive M2 macrophages could serve as biomarkers for post-chemotherapy tumor relapse, we used a 4T1 mouse model treated with CTX. In a pilot study, 4T1 tumor-bearing mice were treated with multiple doses of CTX (75 mg/kg, on days 0, 3, 6, and 9). On day 20, 4T1 tumors began to relapse after CTX treatment (**Figure S1A**). During the CTX treatment, we performed flow cytometry analysis to determine the levels of CD206$^+$F4/80$^+$ M2 macrophages. Although the population of M2 macrophages in tumors at day 8 (a time point at which tumors did not relapse) after CTX treatment was comparable to that at day 0, a significant increase in M2 macrophage recruitment was observed on day 16 (a time point close to the time at which tumors began to relapse [day 20]; **Figure S1B**). This pilot study suggested that increased recruitment of CD206$^+$F4/80$^+$ M2 macrophages may be an early biomarker before tumor relapse.

To further validate our pilot study, we treated 4T1 tumor-bearing mice with either a single dose or multiple doses of CTX (**Figure 1A**). A single dose of CTX (CTX-S; 150 mg/kg, once on day 0) did not inhibit tumor growth, and tumors relapsed from day 10 (**Figure 1B**). In contrast, tumors in mice receiving multiple doses of CTX (CTX-M; 75 mg/kg, every 3 days for 6 times) did not show evident relapse up to 22 days (**Figure 1B**). We next evaluated the phenotypes of macrophages that were recruited to the tumors by flow cytometry on day 8 (a time point close to the time at which tumors will soon relapse in the CTX-S group, but not in the CTX-M group). In both the CTX-S and CTX-M groups, the number of CD206$^-$F4/80$^+$ cells significantly increased compared to that of the control tumors (**Figure 1C, D**). However, the number of CD206$^+$F4/80$^+$ M2 macrophages increased in tumors treated with CTX-S but not in tumors treated with CTX-M (**Figure 1C, E**). The CD206$^+$F4/80$^+$ macrophage-to-CD206$^-$F4/80$^+$ cell ratio was also significantly higher in the CTX-S group compared to CTX-M group (1.16 ± 0.35 vs. 0.27 ± 0.10, *P* <0.01; **Figure 1F**). Immunofluorescence staining of CD206 and F4/80 showed consistent results with flow cytometry results (**Figure 1G**). The proliferation index based on Ki67 staining was significantly higher in CTX-S tumors compared to CTX-M tumors (32.83 % ± 7.68 % vs. 21.79 % ± 6.57 %, *P* <0.01; **Figure S2**), suggesting there was a relapse potential of CTX-S tumors but not CTX-M tumors. The number of lung metastatic lesions in mice treated with CTX-S was also significantly larger than that treated with CTX-M (9.17

± 2.79 vs. 4.13 ± 1.89, *P* <0.01; **Figure S3**). These results indicated that the recruitment of CD206-positive M2 macrophages into tumors was significantly increased in relapsing tumors (CTX-S), but not in non-relapsing tumors (CTX-M) after CTX treatment, suggesting that CD206^{+} M2 macrophages could be biomarkers for tumor relapse after CTX treatment.

Preparation of CD206-targeting probes and *in vivo* targeting of M2 macrophages

Due to increased M2 macrophage recruitment in relapsed tumors after CTX treatment, we hypothesized that CD206 could serve as a biomarker for post-chemotherapy tumor relapse. Thus, a CD206-targeting probe could be useful for the prediction of post-chemotherapy tumor relapse. Thus, we synthesized two CD206-specific probes for both the NIRF imaging and SPECT/CT after CTX treatment.

The CD206-targeting NIRF imaging probe (Dye-αCD206) was prepared by conjugation of an anti-CD206 monoclonal antibody with the near-infrared dye Dylight755 [16]. The purity of Dye-αCD206 was confirmed using sodium dodecyl sulfate-polyacrylamide gel electrophoresis (SDS-PAGE) and NIRF imaging (**Figure S4**). [125]I radiolabeled anti-CD206 antibody (^{125}I-αCD206) was synthesized as a CD206-specific radiotracer for SPECT. After purification, ^{125}I-αCD206 exhibited high radiochemical purity (**Figure S5**). The specific binding capacity of ^{125}I-αCD206 was confirmed by an *in vitro* binding study using CD206^{+} RAW264.7 cells [16] (**Figure S6**).

To investigate the M2 macrophage targeting of the NIRF imaging probe *in vivo*, 4T1 tumor-bearing mice were administered either Dye-αCD206 or Dye-IgG by i.v. injection. Mice were NIRF-imaged at different time points after injection (**Figure S7A**). Tumor uptake of Dye-αCD206 was significantly higher than that of Dye-IgG at all time points examined (**Figure S7B**), suggesting CD206-specific targeting of Dye-αCD206. Optical imaging has inherent limitations in data quantification and imaging of deep tissues. We therefore validated the NIRF results by performing SPECT imaging and radiotracer-based biodistribution analysis using the counterparts of ^{125}I-αCD206 and ^{125}I-IgG. Representative SPECT/CT images are presented in **Figure S8**. Markedly higher tumor accumulation was observed in mice injected with ^{125}I-αCD206 compared to those injected with ^{125}I-IgG. The biodistribution results also showed that ^{125}I-αCD206 tumor uptake
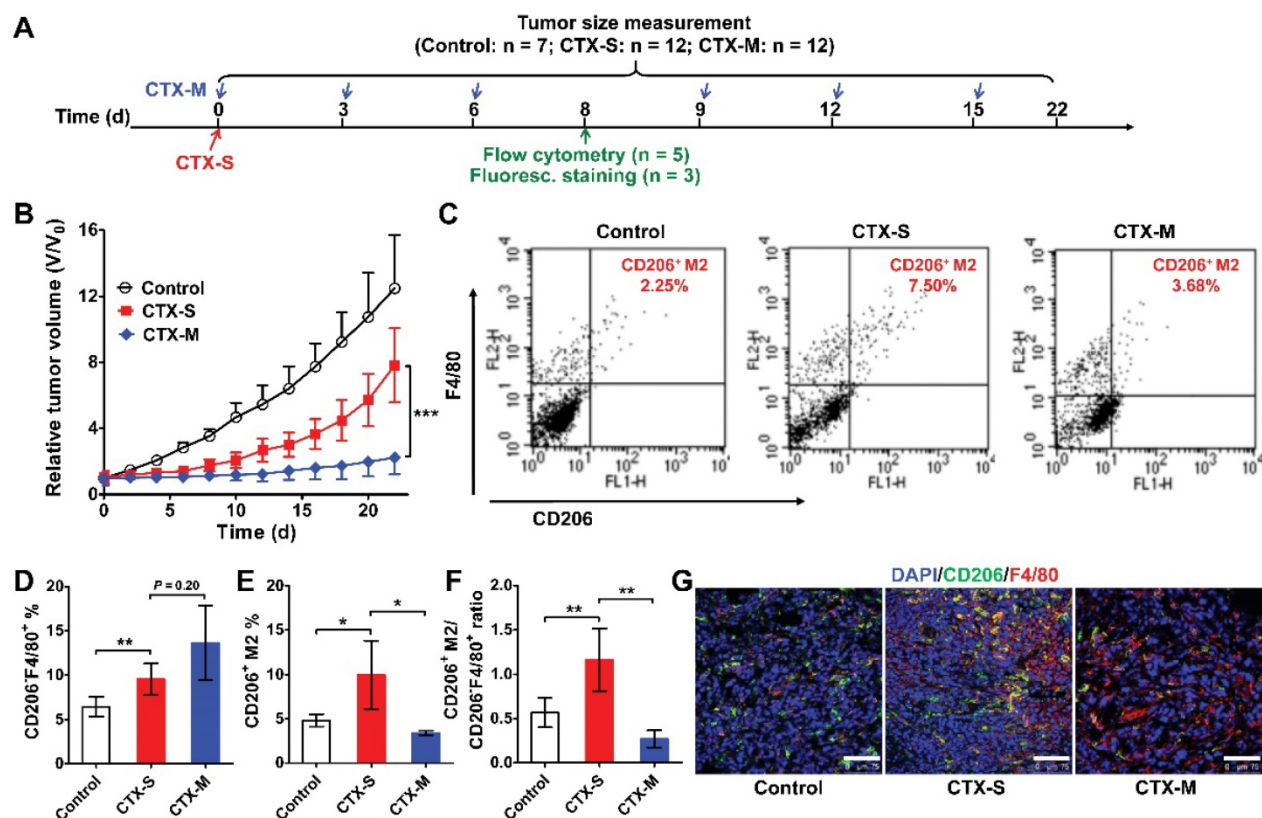

Figure 1. M2 macrophage recruitment increased in relapse-prone tumors after a single dose of CTX treatment. (A) Schedule of CTX treatment. (B) Tumor growth curves of 4T1 tumor-bearing mice treated with PBS (control, n = 7) and different doses of CTX; CTX-S (single dose, 150 mg/kg, n = 12), CTX-M (multiple doses, 75 mg/kg, every 3 days, six times, n = 12); (C-F) Representative dot plots (C), quantified CD206·F4/80^{+} and CD206^{+}F4/80^{+} cell percentages (D, E), and CD206^{+}F4/80^{+}-to-CD206·F4/80^{+} ratios (F) from flow cytometry analysis of CD206 and F4/80 in 4T1 tumors treated with different doses of CTX (n = 5 per group). (G) Immunofluorescence staining of CD206 and F4/80 in 4T1 tumor tissues after PBS and CTX treatments. Scale, 75 μm. *, *P* <0.05; **, *P* <0.01; ***, *P* <0.001.

was significantly higher compared to that of ^{125}I-IgG at 24 h p.i. (4.47 %ID/g ± 1.80 %ID/g vs. 1.81 %ID/g ± 0.39 %ID/g, *P* <0.05; **Figure S9**). Notably, CD206 is expressed in several normal organs such as the liver and lung [29, 30], which might partially explain the higher uptake of ^{125}I-αCD206 compared to ^{125}I-IgG in these organs. The tumor-to-muscle ratio of ^{125}I-αCD206 was also significantly higher than that of ^{125}I-IgG (*P* <0.05; **Figure S9**). These results suggested that our probes could specifically target CD206 in 4T1 tumors. Taken together, our CD206-targeting NIRF imaging and SPECT probes could be used for *in vivo* visualization of CD206^{+} M2 macrophage infiltration in 4T1 tumor-bearing mice.

NIRF and SPECT/CT reveal higher M2 macrophage infiltration in relapse-prone tumors

We next investigated whether M2 macrophage recruitment in relapse-prone tumors after CTX treatment could be visualized *in vivo* using NIRF imaging and SPECT/CT. CTX treatment was started on day 0, and NIRF and SPECT/CT imaging studies were performed on days 7 and 8, respectively (**Figure 2A**). Representative NIRF images obtained in mice administered different doses of CTX were examined 24 h after Dye-αCD206 injection (**Figure 2B**). The fluorescence intensity of Dye-αCD206 in subcutaneous tumors was significantly higher in relapsing CTX-S mice than in non-relapsing CTX-M mice (11.21 %Flu ± 5.05 %Flu vs. 4.26 %Flu ± 0.35 %Flu, *P* <0.01, **Figure 2C**). In our pilot study, 4T1 tumor-bearing mice were treated with multiple doses of CTX and NIRF imaging results showed that the tumor uptake of Dye-αCD206 on day 8 (a time point at which tumors will not relapse soon) was comparable to that on day 0. In contrast, a significant increase in tumor uptake of Dye-αCD206 was observed on day 16 (a time point at which tumors will relapse soon) as compared to that on day 0 (*P* <0.01; **Figure S10**).
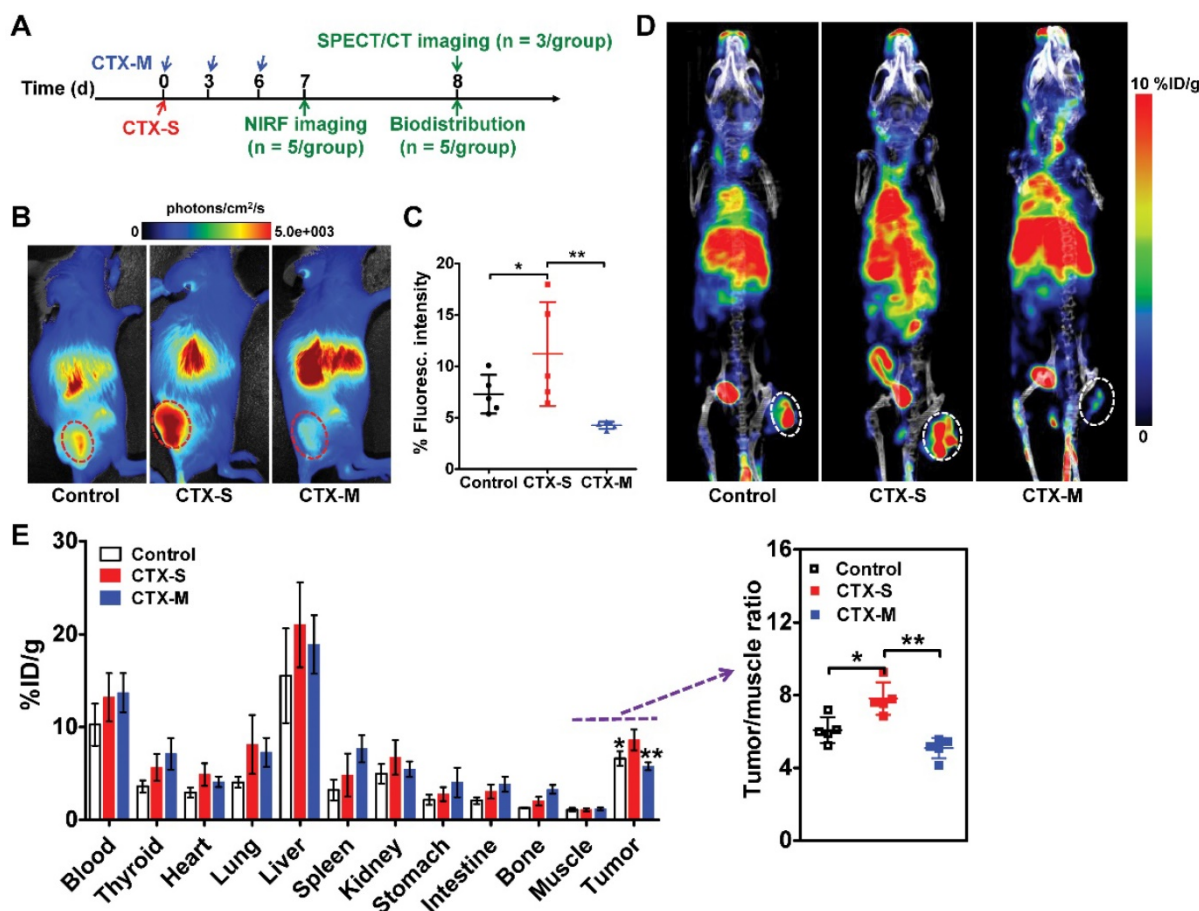

Figure 2. Significantly increased uptake of Dye-αCD206 and ^{125}I-αCD206 in 4T1 tumors treated with a single dose of CTX, as determined by NIRF and SPECT/CT imaging. (A) Schedule of NIRF and SPECT/CT imaging. (B-C) Representative NIRF images (B) and quantified tumor uptake (C) of control (PBS), CTX-S (single dose, 150 mg/kg) and CTX-M (multiple doses, 75 mg/kg, every 3 days, three times) treated mice 24 h after Dye-αCD206 injection (n = 5 per group). (D) Representative SPECT/CT images of control, CTX-S-, and CTX-M-treated mice 24 h after ^{125}I-αCD206 injection. (E) Biodistribution of ^{125}I-αCD206 in major organs and tumors (n = 5 per group). Inset, results of the tumor-to-muscle ratios of ^{125}I-αCD206. Tumors are indicated with circles. *, *P* <0.05; **, *P* <0.01.
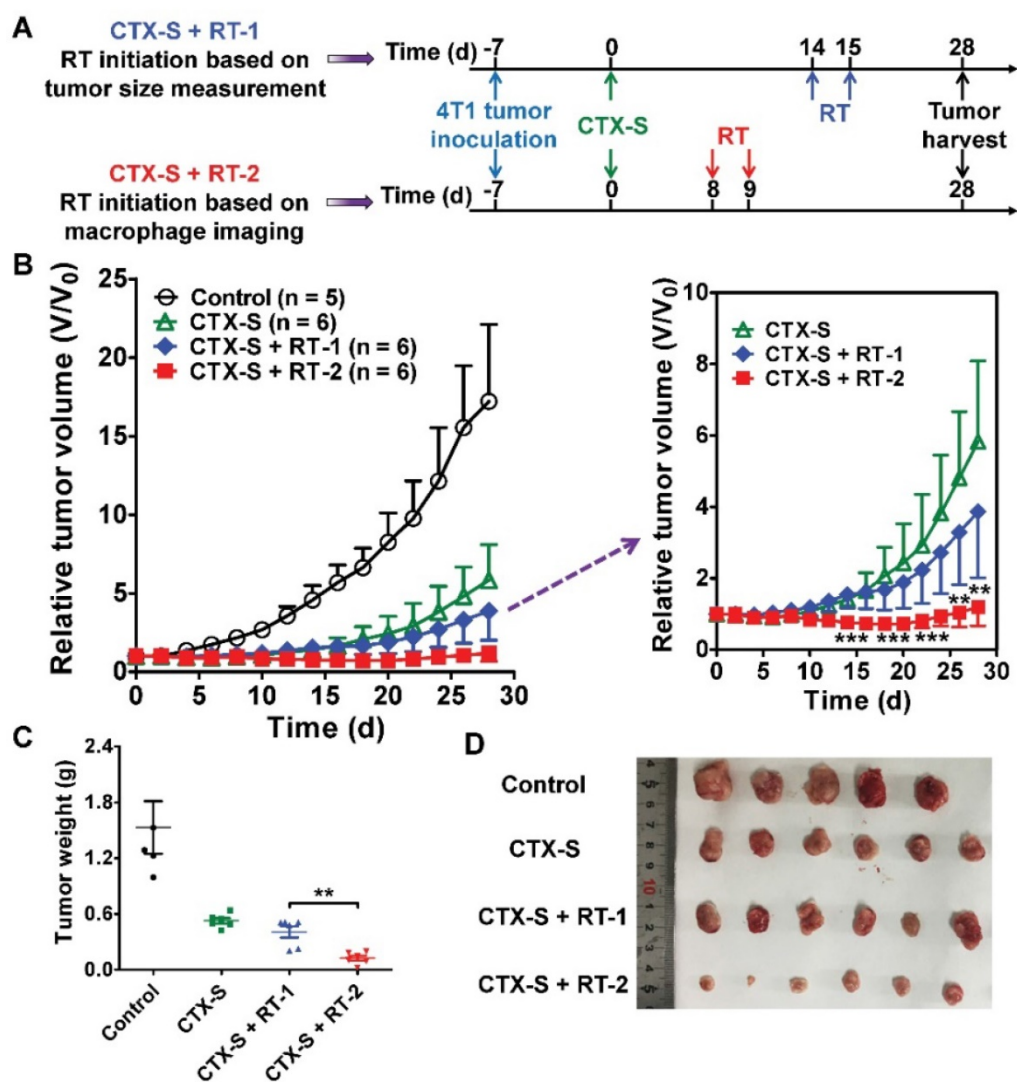
Figure 3. Initiation of additional radiotherapy (RT) based on molecular imaging of M2 macrophages leads to significantly improved tumor suppression. (A) Schematic illustration showing the design of CTX and RT combination therapy (Control, n = 5; CTX-S, n = 6; CTX-S + RT-1, n = 6; CTX-S + RT-2, n = 6). (B) 4T1 tumor growth curves after combination therapy. (C-D) Tumor weights (C) and photographs (D) from 4T1 tumor-bearing mice on day 28 after the indicated treatments. **, *P* <0.01; ***, *P* <0.001.

NIRF imaging results were validated by SPECT/CT and biodistribution analyses. As shown in **Figure 2D**, the probe showed markedly increased accumulation in CTX-S tumors compared to CTX-M tumors at 24 h after ^{125}I-αCD206 injection. The calculated tumor uptake of ^{125}I-αCD206 was significantly higher in the CTX-S group than that in the CTX-M group (8.60 %ID/g ± 1.12 %ID/g vs. 5.77 %ID/g ± 0.43 %ID/g, *P* <0.01; **Figure 2E**). The tumor-to-muscle ratio of ^{125}I-αCD206 was also significantly higher in the CTX-S group than that in the CTX-M group (*P* <0.01; **Figure 2E**). These results indicated that *in vivo* imaging of CD206+ M2 macrophages could be used to predict tumor early relapse after CTX treatment.

Early prediction of tumor relapse by molecular imaging of CD206+ M2 macrophages facilitates effective tumor therapy upon additional radiotherapy

Noninvasive NIRF and SPECT imaging of the enhanced CD206-positive M2 macrophage infiltration on days 7 and 8 successfully predicted tumor relapse after CTX-S treatment (**Figure 2**; **Figure 1B**). We then investigated whether early prediction of tumor relapse by molecular imaging of CD206+ M2 macrophages could facilitate an improved tumor management. We initiated additional radiotherapy in the CTX-S-treated 4T1 tumor-bearing mice (**Figure 3A**) either on day 8 (tumor relapse predicted by NIRF and SPECT/CT imaging) or on day 14 (tumor relapse determined by a measured and statistically significant increase in tumor size in comparison to that on day 0;

Figure 3B). The 4T1 tumors were locally irradiated with 6 Gy two consecutive days starting on days 8 and 14, respectively (**Figure 3A**). Tumor growth in the group of additional radiotherapy starting on day 14 (CTX-S + RT-1 group) was partially inhibited compared to that in the CTX-S group. In contrast, additional radiotherapy starting on day 8 (CTX-S + RT-2 group) caused an almost complete elimination of 4T1 tumors, and the average tumor size did not change until the end of the study (**Figure 3B**). On day 28, the average tumor weight of CTX-S + RT-2 group was significantly lower than that in the CTX-S + RT-1 group (*P* <0.01; **Figure 3C, D**). These results indicate that early prediction of tumor relapse by molecular imaging of CD206+ M2 macrophages facilitates an improved tumor management upon additional combination therapy.

M2 macrophages promote tumor relapse and lung metastasis after chemotherapy

To further investigate the role of M2 macrophages in tumor growth and metastasis, we isolated F4/80+CD206+ M2 macrophages from tumors treated with a single dose of CTX by FACS. Isolated macrophages were transplanted into tumors treated with multiple doses of CTX (75 mg/kg, every three days, four times) by intratumoral injection (**Figure 4A**). Tumors transplanted with M2 macrophages showed accelerated relapse compared to control tumors without macrophage transplantation (**Figure 4B**). A significant difference in tumor regrowth was observed from day 12 to day 22 (**Figure 4B**). Ki67 staining showed increased tumor cell proliferation in macrophage-transplanted tumors (CTX-M + M2 Mφ) compared to tumors without macrophage transplantation (CTX-M group; **Figure 4C**). The proliferation index was significantly higher in macrophage-transplanted tumors compared to non-macrophage transplanted tumors (43.22 % ± 8.23 % vs. 22.82 % ± 5.71 %, *P* <0.001, **Figure 4D**). These results indicated that CD206+ M2 macrophages promoted tumor relapse after CTX treatment.

TAMs facilitate tumor metastasis by promoting extravasation, survival and growth of metastatic tumor cells [3, 31]. Subcutaneous 4T1 tumors can lead to metastasis at distant sites such as the lungs [11, 16]. Therefore, we assessed the metastatic promotion effect of CD206+ M2 macrophages in CTX-treated mice by performing an adoptive macrophage transfer study. As shown in **Figure 4E, F**, there were significantly greater numbers of metastatic lung lesions in mice with M2 macrophage transplantation compared to that without transplantation (35.00 ± 23.52 vs. 5.25 ± 3.40, *P* <0.05). Metastatic lesion counting results were validated by histological H&E staining examinations (**Figure 4G**). These findings suggested that M2 macrophages promoted lung metastasis of 4T1 tumors after CTX treatment.
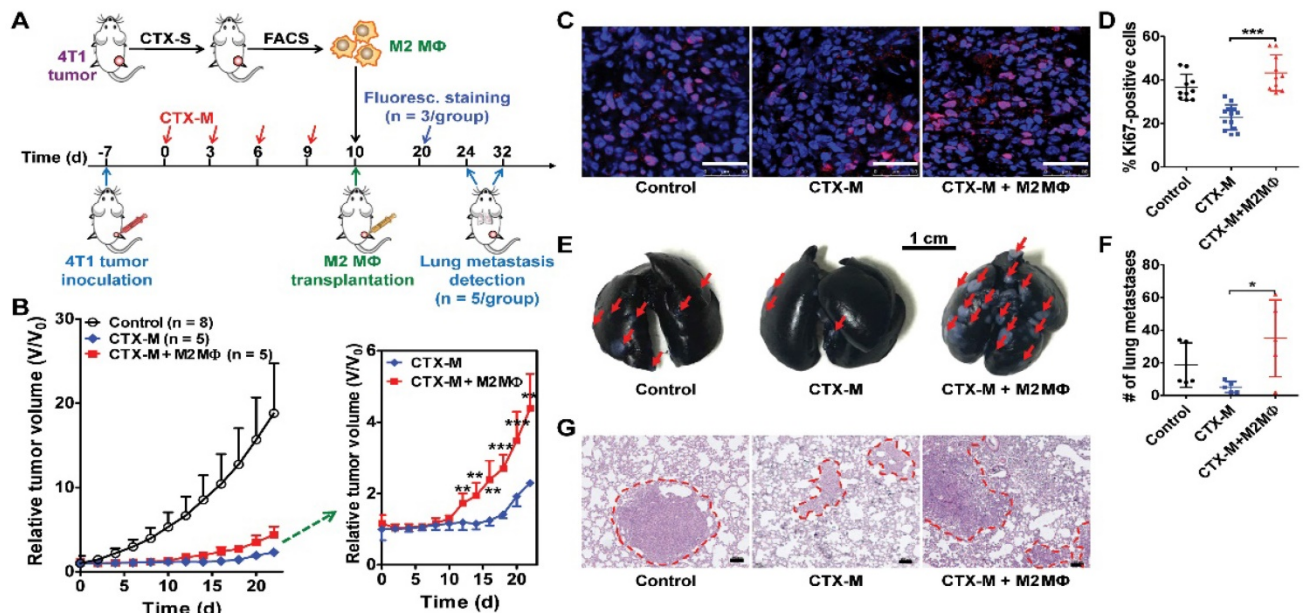

Figure 4. M2 macrophages promote tumor relapse and metastasis after multiple doses of CTX treatment (CTX-M; 75 mg/kg, every 3 days, four times). (A) Schematic illustration of CTX treatment and adoptive M2 macrophage (Mφ) transfer. (B) Post-CTX-M treatment 4T1 tumor regrowth after M2 macrophage transplantation (Control, n = 8; CTX-M, n = 5; CTX-M + M2 Mφ, n = 5). (C) Immunofluorescence staining of Ki67 in 4T1 tumor tissues after the indicated treatments (on day 20). Scale, 50 μm. (D) Quantitative analysis of Ki67-positive cells shown in panel C. (E-G) Representative images from India-ink filled lungs (E; scale, 1 cm), quantitative analysis of metastatic lesions (n = 5 per group) (F), and H&E staining (G; scale, 100 μm) of lung sections of 4T1 tumor-bearing mice after the indicated treatments (on day 24 for control group and day 32 for CTX-treated groups). Metastatic lesions are indicated with arrows and dashed circles. *, *P* <0.05; **, *P* <0.01; ***, *P* <0.001.

Depletion of M2 macrophages slows tumor relapse after chemotherapy

As M2 macrophages promote tumor relapse after CTX treatment, M2 macrophage depletion could potentially inhibit tumor relapse. Zoledronic acid (ZA) has been approved for the treatment of cancer-induced bone disease [32]. ZA reduces the number of TAMs and impairs their M2-like polarization, reducing tumor growth and metastasis [32-34]. ZA not only causes M2 macrophage depletion, but can also lead to M2-to-M1 macrophage repolarization [11, 33, 35]. We thus investigated the combination effect of CTX (single dose, 150 mg/kg, once) and ZA in 4T1 tumor-bearing mice. After 2 weeks of combination therapy, mice treated with ZA only did not display inhibition of tumor growth compared to the control group, consistent with previous reports [11]. However, tumor relapse was significantly suppressed with combination therapy of ZA plus CTX compared to CTX only (**Figure S11**). During combination therapy, representative small animal NIRF images showed decreased tumor uptake of Dye-αCD206 in the combination therapy group compared to the CTX-treated group (5.26 %Flu ± 2.21 %Flu vs. 9.30 %Flu ± 1.14 %Flu, P <0.05, **Figure S12A, B**). Tumor uptake in the ZA-treated group was also lower than that in the control group (6.32 %Flu ± 0.46 %Flu vs. 8.01 %Flu ± 0.93 %Flu, P <0.01, **Figure S12A, B**), consistent with the M2 macrophage depletion effect of ZA. These results indicated that M2 macrophage depletion inhibits the progression of tumor relapse after CTX treatment in 4T1 tumor-bearing mice, and it could be visualized using CD206-targeting NIRF imaging.

In vivo targeting of CD206+ macrophages in lymphatic metastasis

M2 macrophages play an important role not only in the progression and proliferation of tumor cells but also in tumor metastasis [31]. Recent studies showed that M2 macrophages correlate with lymph node and distant metastases [36, 37]. We therefore investigated whether M2 macrophage recruitment could be visualized using our CD206-targeting probes in a 4T1 lymph node metastasis model (**Figure 5A**). We established a 4T1 lymph node metastasis model by inoculation of 4T1-fLuc cells into the right hind footpads of mice. 4T1 tumor cells spread to the right popliteal lymph node as the sentinel lymph node. As shown in **Figure 5B**, tumor growth was observed using BLI from day 7 to day 21. Results showed primary tumor growth, but no signal in tumor-draining popliteal lymph nodes. At day 21, *ex vivo* BLI of both sides of the popliteal lymph nodes confirmed 4T1 tumor metastasis in the right popliteal

lymph nodes (**Figure 5B**). We then used Dye-αCD206 as a small animal NIRF imaging probe. *In vivo* NIRF imaging results showed no obvious signal of tumor-draining lymph nodes. However, when the popliteal lymph nodes were exposed by surgery, these showed a higher uptake compared to that of the control contralateral lymph nodes (**Figure 5C**). *Ex vivo* NIRF imaging results showed higher uptake of Dye-αCD206 in tumor-draining lymph nodes compared to control lymph nodes. The metastatic lymph node-to-non-metastatic lymph node uptake ratio of Dye-αCD206 was also significantly higher than that of Dye-IgG (P <0.05; **Figure 5D**).

NIRF imaging results were validated using SPECT/CT by injection of ^{125}I-αCD206. Compared to NIRF imaging, SPECT is a non-invasive imaging method that is not limited by tissue depth. Tumor-draining lymph nodes could be visualized non-invasively using SPECT/CT. Performance of *ex vivo* SPECT/CT after removal of the bilateral popliteal lymph nodes confirmed the *in vivo* SPECT/CT results. The uptake of ^{125}I-αCD206 in tumor-draining lymph nodes was markedly higher compared to that of the control contralateral lymph nodes (**Figure 5E**). Histological examination based on H&E staining confirmed metastasis in tumor-draining popliteal lymph nodes (**Figure 5F**). Immunofluorescence staining of CD206 showed higher immunoreactivity and co-localization in tumor-draining lymph nodes, but not in the contralateral control lymph nodes, confirming CD206-positive M2 macrophage recruitment in the tumor-draining lymph nodes (**Figure 5F**). These results suggested that M2 macrophages were recruited to metastatic lymph nodes and could be visualized by NIRF imaging and SPECT/CT using CD206-targeted probes.

Discussion

Post-chemotherapy tumor relapse is a severe problem in clinical oncology, since it usually involves inoperable metastatic disease and complications. Early detection of key biomarkers that could potentially predict tumor recurrence could lead to improved outcomes in cancer patients by providing opportunities for better treatment and prevention. Key biomarkers, as determined from biopsy or peripheral blood specimens, have a high predictive value. However, they have major limitations of being either invasive, having limited quantitative value, or not providing whole-body information regarding disease progression. In this study, we described a noninvasive and dynamic method of whole-body imaging to sensitively detect tumor relapse at the early stage after chemotherapy and tumor lymph metastasis using NIRF or SPECT imaging of CD206

expression in tumor-infiltrated M2 macrophages.

Small-animal NIRF and SPECT/CT imaging demonstrated that molecular imaging of M2 macrophages by targeting CD206 could predict tumor relapse post-CTX treatment in an earlier manner (day 7 or 8 vs. day 10; **Figure 2B, D**; **Figure 1B**) than that based on the observed increase in tumor size. The dynamic readout of changes in M2 macrophages would open up the possibility for early assessment of tumor responses to chemotherapy. In clinical practice, combination therapy is usually needed to overcome tumor recurrence after chemotherapy [38]. However, key issues in combination therapy include how to rationally design combination regimens for a more efficacious outcome. As a proof-of-concept, we showed that early prediction of tumor relapse by molecular imaging of M2 macrophages resulted in a significantly improved tumor suppression upon early initiation of additional radiotherapy in comparison to that determined by measurement of tumor size. These results demonstrate the potential role of M2 macrophage-targeted molecular imaging for patient stratification and dose optimization.

In this study, we used Dye- and ^{125}I-labeled intact anti-CD206 antibody for noninvasive imaging of M2 macrophage infiltration in subcutaneous and lymph node metastatic 4T1 tumor models. Intact antibodies, due to their high molecular weight (~150 kDa), have long circulating half-life, resulting in high background accumulation *in vivo*, limiting their wide applications for clinical use [39, 40]. Further optimization of the CD206-targeted imaging agents such as using antibody fragments or nanobodies is needed for clinical application. In addition, the antibody used in this study is a rat IgG anti-mouse CD206. Since different species of antibodies have various *in vivo* pharmacokinetics in different species, further studies testing humanized anti-CD206 antibodies in different animal models such as orthotopic model, patient-derived xenograft tumor models, or even transgenic models may be needed to further validate the results of this study. Another limitation of our study is that we could not reflect on the spatial distribution of M2 macrophages by simply using NIRF imaging and a biodistribution study, as macrophages infiltrated in tumors are not homogeneous [2]. Macrophages in different locations might have different impacts on tumor progression and invasion [41, 42]. To overcome this, analyzing macrophage microdistribution using high-resolution SPECT or PET might be needed to more accurately investigate the correlation between macrophage infiltration and tumor progression.
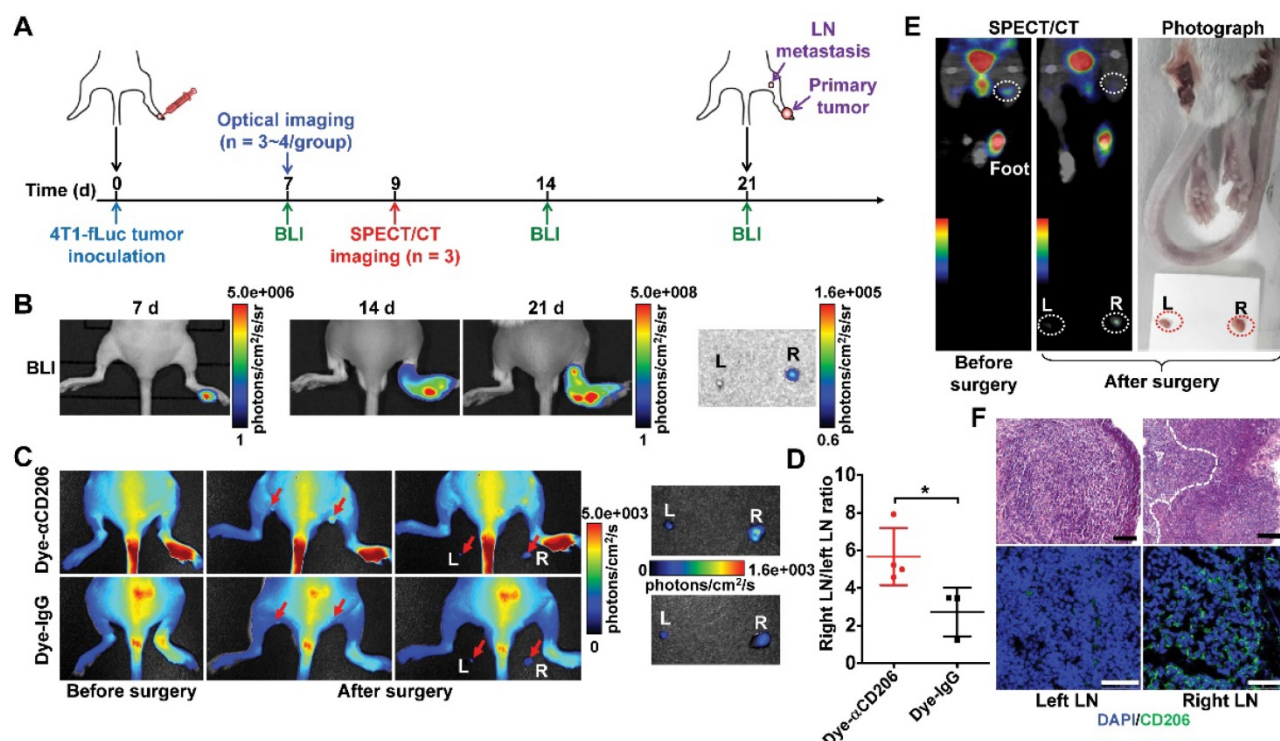

Figure 5. Detection of tumor lymphatic metastases by NIRF and SPECT/CT imaging of M2 macrophages. (A) Schematic illustration of 4T1 lymph node metastasis imaging experiments. (B) BLI results of 4T1 lymph node metastasis model (on days 7, 14, and 21). (C) Representative *in vivo* NIRF images and *ex vivo* images after surgery of 4T1 lymph node metastasis 24 h after Dye-αCD206 or Dye-IgG injection. Popliteal lymph nodes are indicated with arrows. (D) Quantified right lymph node (LN)-to-left LN uptake ratios of Dye-αCD206 (n = 4) and Dye-IgG (n = 3). (E) SPECT/CT of 4T1 lymph node metastasis before and after surgery 24 h after ^{125}I-αCD206 injection. Popliteal lymph nodes are indicated with circles. (F) Histological analysis of H&E staining (scale, 100 μm) and immunofluorescence staining (scale, 50 μm) of CD206 in bilateral popliteal lymph node sections from 4T1 lymph node metastatic mice. *, *P* <0.05.

Several other probes that have been reported for *in vivo* targeting of CD206 [11-13, 43]. [99mTc]-Tilmanocept, which has been approved for mapping the sentinel lymph node in patients with breast cancer and melanoma, is a [99mTc]-labeled mannosyl-dextran macromolecule, in which the mannose acts as a ligand for the CD206 receptor [43]. Most of the preclinical and clinical use of [99mTc]-Tilmanocept is limited to lymph node mapping through peritumoral or intradermal injection for its rapid clearance, high sentinel node and low distal node accumulation [43, 44]. The applications of [99mTc]-Tilmanocept by systemic administration for noninvasive imaging of macrophage infiltration into tumors are rare; one of the possible reasons is that the affinity of mannose to CD206 is generally limited in comparison to CD206-specific antibodies. A CD206-specific nanobody has also been recently reported for *in vivo* imaging of M2 macrophages in tumors and macrophages in joint inflammation [12, 13]. The relatively small molecular weight of nanobody confers its rapid circulation clearance and high contrast for macrophage-targeted imaging, which guarantees its further application for molecular imaging of macrophages in guiding cancer therapy and monitoring metastasis.

The tumor invasion- and metastasis-promoting effects of M2 macrophages have been reported in several studies [31, 36, 37] and verified in our adoptive M2 macrophage transfer as well as ZA-based macrophage depletion experiments. The first step of metastasis often occurs in the sentinel lymph nodes [45]. Clinically, lymph node metastases in patients are tested by histological analysis in lymph node tissues dissected from patients, which is accurate but invasive and complicated [46]. We address this issue in this study by testing CD206-targeting probes for the noninvasive imaging of lymph node metastasis in a 4T1 lymph node metastasis model. Tumor metastases in tumor-draining lymph nodes could be visualized by NIRF and SPECT imaging of CD206. Different from [99mTc]-Tilmanocept, which was peritumorally or intradermally injected for sentinel lymph node detection, our CD206-targeted probes were administered by intravenous injection. The low uptake of the systemically injected imaging probes in the CD206-positive macrophages together with the small population of CD206-positive macrophages in the lymph node, as well as the limitation of planar optical imaging for deep tissue imaging may explain why NIRF imaging could enable observation of tumor-draining lymph nodes only by exposing them by surgery. Future studies investigating the local injection of our probes may be needed to further increase the imaging signals for metastatic lymph node detection.

It is well-recognized that tumors often drive strong inflammation and induce infiltration of inflammatory cells, and this phenomenon is observed in both the original tumor and tumor-draining lymph nodes (TDLNs) [47]. By NIRF imaging in a dual inflammation and 4T1 tumor mouse model, we demonstrated that both Dye-αCD206 and Dye-IgG exhibited comparable high uptake in the inflamed tissue. In contrast, the 4T1 tumor uptake of Dye-αCD206 was significantly higher than that of Dye-IgG (**Figure S13A, B**). Immunofluorescence staining of the inflamed tissue showed the absence of CD206- or F4/80-positive cells (**Figure S13C**). Therefore, the high uptake of Dye-αCD206 in the inflamed tissue was most likely due to the enhanced vascular permeability and blood perfusion (i.e., enhanced permeability and retention [EPR] effect) in the inflamed tissue. Recent studies demonstrated that metastatic lymph nodes express much higher levels of CD206 than the non-metastatic lymph nodes [44]. Moreover, a recent study examining human pancreatic cancer samples suggested that M2 macrophages infiltrate the sentinel lymph node earlier than metastatic tumor cells [48]. These results indicate that in comparison to nonspecific imaging agents such as [18F]-FDG, CD206-targeted imaging probes hold promise for specifically detecting metastatic lymph nodes in an early manner. Notably, control studies using nonspecific agents such as IgG may be needed to exclude the possibility of nonspecific targeting due to the EPR effect of inflammation in the metastatic lymph nodes.

It is noteworthy that CD206 is expressed not only on M2 macrophages, but also on dendritic cells (DCs) [43]. Chemotherapy did not increase the recruitment of DCs into tumors [2]. Therefore, in our subcutaneous 4T1 mouse model, the significantly increased tumor imaging signals of NIRF and radiolabeled CD206-targeting probes used in this study after CTX therapy are impossibly due to their specific targeting to DCs, but only to M2 macrophages. However, DCs may infiltrate into the inflammatory lymph nodes in the tumor situation [49]. Therefore, in our lymph node metastatic model, further studies may be needed to demonstrate the specific location of CD206-targeted probes in M2 macrophages, DCs, or in both.

Conclusions

Our study demonstrated that M2 macrophage accumulation in tumors promoted post-chemo-therapy tumor relapse and distant metastasis, and M2 macrophage depletion slowed tumor relapse after

chemotherapy. CD206-targeted NIRF imaging and SPECT enables noninvasive visualization of M2 macrophage recruitment into tumors and metastatic lymph nodes. Moreover, early prediction of tumor relapse by molecular imaging of M2 macrophages facilitates an improved tumor management upon additional radiotherapy. Taken together, CD206-targeted molecular imaging of M2 macrophages could potentially be used to predict and evaluate tumor relapse and metastasis after chemotherapy, and to aid in the rational design of effective combination therapy in the clinic.

Abbreviations

NIRF: near-infrared fluorescence; SPECT: single-photon emission computed tomography; TAM: tumor-associated-macrophage; MMR: macrophage mannose receptor; PET: positron emission tomography; 4T1-fLuc: firefly luciferase stably-transfected 4T1; BLI: bioluminescence imaging; CTX: cyclophosphamide; PBS: phosphate buffered solution; PE: phycoerythrin; FITC: fluorescein isothiocyanate; αCD206: anti-CD206 antibody; p.i.: postinjection; i.v.: intravenously; %ID/g: percentage of the injected dose per gram of tissue; H&E: hematoxylin and eosin; CTX-S: single dose of CTX; CTX-M: multiple doses of CTX; SDS-PAGE: sodium dodecyl sulfate-polyacrylamide gel electrophoresis; %Flu: % fluorescence intensity; ZA: zoledronic acid; TDLN: tumor-draining lymph node; EPR: enhanced permeability and retention; DC: dendritic cell; ITLC: instant thin-layer chromatography.

Supplementary Material

Supplementary methods and figures.
http://www.thno.org/v07p4276s1.pdf

Competing Interests

The authors have declared that no competing interest exists.

References

1. Chambers AF, Groom AC, MacDonald IC. Dissemination and growth of cancer cells in metastatic sites. Nat Rev Cancer. 2002; 2: 563-72.
2. Hughes R, Qian BZ, Rowan C, et al. Perivascular M2 macrophages stimulate tumor relapse after chemotherapy. Cancer Res. 2015; 75: 3479-91.
3. Noy R, Pollard JW. Tumor-associated macrophages: from mechanisms to therapy. Immunity. 2014; 41: 49-61.
4. Schroeder A, Heller DA, Winslow MM, et al. Treating metastatic cancer with nanotechnology. Nat Rev Cancer. 2011; 12: 39-50.
5. Junttila MR, de Sauvage FJ. Influence of tumour micro-environment heterogeneity on therapeutic response. Nature. 2013; 501: 346-54.
6. De Palma M, Lewis CE. Macrophage regulation of tumor responses to anticancer therapies. Cancer Cell. 2013; 23: 277-86.
7. Biswas SK, Mantovani A. Macrophage plasticity and interaction with lymphocyte subsets: cancer as a paradigm. Nat Immunol. 2010; 11: 889-96.
8. Bingle L, Brown NJ, Lewis CE. The role of tumour-associated macrophages in tumour progression: implications for new anticancer therapies. J Pathol. 2002; 196: 254-65.
9. Choi KM, Kashyap PC, Dutta N, et al. CD206-positive M2 macrophages that express heme oxygenase-1 protect against diabetic gastroparesis in mice. Gastroenterology. 2010; 138: 2399-409, 409 e1.
10. Allavena P, Chieppa M, Bianchi G, et al. Engagement of the mannose receptor by tumoral mucins activates an immune suppressive phenotype in human tumor-associated macrophages. Clin Dev Immunol. 2010; 2010: 547179.
11. Sun X, Gao D, Gao L, et al. Molecular imaging of tumor-infiltrating macrophages in a preclinical mouse model of breast cancer. Theranostics. 2015; 5: 597-608.
12. Put S, Schoonooghe S, Devoogdt N, et al. SPECT imaging of joint inflammation with nanobodies targeting the macrophage mannose receptor in a mouse model for rheumatoid arthritis. J Nucl Med. 2013; 54: 807-14.
13. Movahedi K, Schoonooghe S, Laoui D, et al. Nanobody-based targeting of the macrophage mannose receptor for effective in vivo imaging of tumor-associated macrophages. Cancer Res. 2012; 72: 4165-77.
14. Luo Y, Zhou H, Krueger J, et al. Targeting tumor-associated macrophages as a novel strategy against breast cancer. J Clin Invest. 2006; 116: 2132-41.
15. Zhang W, Zhu XD, Sun HC, et al. Depletion of tumor-associated macrophages enhances the effect of sorafenib in metastatic liver cancer models by antimetastatic and antiangiogenic effects. Clin Cancer Res. 2010; 16: 3420-30.
16. Zhang C, Gao L, Cai Y, et al. Inhibition of tumor growth and metastasis by photoimmunotherapy targeting tumor-associated macrophage in a sorafenib-resistant tumor model. Biomaterials. 2016; 84: 1-12.
17. DeNardo DG, Brennan DJ, Rexhepaj E, et al. Leukocyte complexity predicts breast cancer survival and functionally regulates response to chemotherapy. Cancer Discov. 2011; 1: 54-67.
18. Chen L, Li J, Wang F, et al. Tie2 expression on macrophages is required for blood vessel reconstruction and tumor relapse after chemotherapy. Cancer Res. 2016; 76: 6828-38.
19. Ahn GO, Tseng D, Liao CH, et al. Inhibition of Mac-1 (CD11b/CD18) enhances tumor response to radiation by reducing myeloid cell recruitment. Proc Natl Acad Sci U S A. 2010; 107: 8363-8.
20. Weissleder R. Molecular imaging: exploring the next frontier. Radiology. 1999; 212: 609-14.
21. Margolis DJ, Hoffman JM, Herfkens RJ, et al. Molecular imaging techniques in body imaging. Radiology. 2007; 245: 333-56.
22. Gao L, Zhang C, Gao D, et al. Enhanced anti-tumor efficacy through a combination of integrin alphavbeta6-targeted photodynamic therapy and immune checkpoint inhibition. Theranostics. 2016; 6: 627-37.
23. Mumprecht V, Honer M, Vigl B, et al. In vivo imaging of inflammation- and tumor-induced lymph node lymphangiogenesis by immuno-positron emission tomography. Cancer Res. 2010; 70: 8842-51.
24. Liu Z, Yu Z, He W, et al. In-vitro internalization and in-vivo tumor uptake of anti-EGFR monoclonal antibody LA22 in A549 lung cancer cells and animal model. Cancer Biother Radiopharm. 2009; 24: 15-24.
25. Gao D, Gao L, Zhang C, et al. A near-infrared phthalocyanine dye-labeled agent for integrin alphavbeta6-targeted theranostics of pancreatic cancer. Biomaterials. 2015; 53: 229-38.
26. Gao L, Liu H, Sun X, et al. Molecular imaging of post-Src inhibition tumor signatures for guiding dasatinib combination therapy. J Nucl Med. 2016; 57: 321-6.
27. Liu Z, Liu H, Ma T, et al. Integrin alphavbeta6-targeted SPECT imaging for pancreatic cancer detection. J Nucl Med. 2014; 55: 989-94.
28. Huang Q, Li F, Liu X, et al. Caspase 3-mediated stimulation of tumor cell repopulation during cancer radiotherapy. Nat Med. 2011; 17: 860-6.
29. Devey L, Ferenbach D, Mohr E, et al. Tissue-resident macrophages protect the liver from ischemia reperfusion injury via a heme oxygenase-1-dependent mechanism. Mol Ther. 2009; 17: 65-72.
30. Misharin AV, Morales-Nebreda L, Mutlu GM, et al. Flow cytometric analysis of macrophages and dendritic cell subsets in the mouse lung. Am J Respir Cell Mol Biol. 2013; 49: 503-10.
31. Qian BZ, Pollard JW. Macrophage diversity enhances tumor progression and metastasis. Cell. 2010; 141: 39-51.
32. Green JR. Antitumor effects of bisphosphonates. Cancer. 2003; 97: 840-7.
33. Veltman JD, Lambers ME, van Nimwegen M, et al. Zoledronic acid impairs myeloid differentiation to tumour-associated macrophages in mesothelioma. Br J Cancer. 2010; 103: 629-41.
34. Rogers MJ, Gordon S, Benford HL, et al. Cellular and molecular mechanisms of action of bisphosphonates. Cancer. 2000; 88: 2961-78.
35. Tsagozis P, Eriksson F, Pisa P. Zoledronic acid modulates antitumoral responses of prostate cancer-tumor associated macrophages. Cancer Immunol Immunother. 2008; 57: 1451-9.
36. Tang X. Tumor-associated macrophages as potential diagnostic and prognostic biomarkers in breast cancer. Cancer Lett. 2013; 332: 3-10.
37. Chen J, Yao Y, Gong C, et al. CCL18 from tumor-associated macrophages promotes breast cancer metastasis via PITPNM3. Cancer Cell. 2011; 19: 541-55.

38. Green JA, Kirwan JM, Tierney JF, et al. Survival and recurrence after concomitant chemotherapy and radiotherapy for cancer of the uterine cervix: a systematic review and meta-analysis. Lancet. 2001; 358: 781-6.

39. Wu AM, Olafsen T. Antibodies for molecular imaging of cancer. Cancer J. 2008; 14: 191-7.

40. Liu Z, Sun X, Liu H, et al. Early assessment of tumor response to gefitinib treatment by noninvasive optical imaging of tumor vascular endothelial growth factor expression in animal models. J Nucl Med. 2014; 55: 818-23.

41. Movahedi K, Laoui D, Gysemans C, et al. Different tumor microenvironments contain functionally distinct subsets of macrophages derived from Ly6C(high) monocytes. Cancer Res. 2010; 70: 5728-39.

42. Lewis CE, Pollard JW. Distinct role of macrophages in different tumor microenvironments. Cancer Res. 2006; 66: 605-12.

43. Surasi D, O'Malley J, Bhambhvani P. 99mTc-Tilmanocept: A novel molecular agent for lymphatic mapping and sentinel lymph node localization. J Nucl Med Technol. 2015; 43: 87-91.

44. Azad AK, Rajaram MV, Metz WL, et al. gamma-Tilmanocept, a new radiopharmaceutical tracer for cancer sentinel lymph nodes, binds to the mannose receptor (CD206). J Immunol. 2015; 195: 2019-29.

45. Detmar M, Hirakawa S. The formation of lymphatic vessels and its importance in the setting of malignancy. J Exp Med. 2002; 196: 713-8.

46. Blanchard DK, Donohue JH, Reynolds C, et al. Relapse and morbidity in patients undergoing sentinel lymph node biopsy alone or with axillary dissection for breast cancer. Arch Surg. 2003; 138: 482-7.

47. Munn DH, Mellor AL. The tumor-draining lymph node as an immune-privileged site. Immunol Rev. 2006; 213: 146-58.

48. Kurahara H, Takao S, Maemura K, et al. M2-polarized tumor-associated macrophage infiltration of regional lymph nodes is associated with nodal lymphangiogenesis and occult nodal involvement in pN0 pancreatic cancer. Pancreas. 2013; 42: 155-9.

49. Segura E, Amigorena S. Inflammatory dendritic cells in mice and humans. Trends Immunol. 2013; 34: 440-5.